RSC Advances

ROYAL SOCIETY OF CHEMISTRY

www.rsc.org/advances

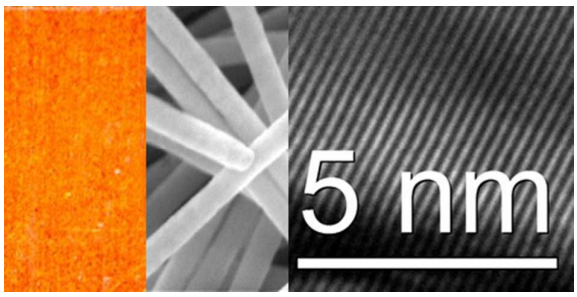

Gold nanowires with controlled crystallinity and preferred crystallographic orientations have been fabricated in ion track-etched templates using a cyanide-free bath.

Cite this: DOI: 10.1039/c0xx00000x

www.rsc.org/xxxxxx

ARTICLE TYPE

Cyanide-free preparation of gold nanowires: controlled crystallinity, crystallographic orientation and enhanced field emission

Shuangbao Lyu,[a,b] Dang Yuan Lei,[c] Wenqiang Liu,[a,b] Huijun Yao,[a] Dan Mo,[a] Yonghui Chen,[a] Peipei Hu,[a,b] Youmei Sun,[a] Jie Liu,*[a] and Jing Lai Duan,*[a]

Received (in XXX, XXX) Xth XXXXXXXXX 20XX, Accepted Xth XXXXXXXXX 20XX
DOI: 10.1039/b000000x

Environment-friendly preparation of nanomaterials with controlled structural features represents a development trend of nanoscience and nanotechnology. In this work, using a cyanide-free bath, gold nanowires with controlled crystallinity and preferred crystallographic orientation have been prepared by electrochemical deposition in home-made polycarbonate ion track-etched templates. Single-crystal and polycrystal gold nanowires with preferred orientations along [111] and [100] directions have been obtained by selecting fabrication parameters, respectively. The influence mechanisms of nanopore diameter, applied voltage, and deposition temperature on structural properties are proposed. In addition, single-crystal nanowires with [100] preferred orientation shows enhanced field emission, which may be attributed to their single-crystal structure and lower work function of loosely packed crystal planes.

1. Introduction

Metallic nanowires (NWs) have attracted significant interest due to their peculiar mechanical, electrical, optical, thermal and magnetic properties in comparison with their bulk counterparts.[1-4] Based on these, various potential applications have been developed in fields such as plasmonics,[5] nanobiotechnology,[6] optics,[7] nanoelectronics,[8] photovoltaics,[9] superconductivity,[10] (photo)catalysis[11,12] and molecular sensing based on Surface Enhanced Raman Scattering.[13,14] Numerous experimental and theoretical studies have confirmed that the physicochemical properties of NWs are considerably determined by their structural characteristics.[15-20] For instance, the magnetic properties of Fe NWs are highly dependent on their crystallinity[18] and the crystallographic orientation of NWs can remarkably influence the thermal expansion properties of Cu NWs.[16] As two dominant structural properties, crystallinity and crystallographic orientation have been a research focus in nanotechnology.

To fabricate NWs, a number of methods have been developed, including template-assisted electrochemical deposition,[21-27] seed-mediated growth,[28] chemical vapour deposition,[29] lithography,[30] hydrothermal reduction[31] and molecular beam epitaxy.[32] Among these methods, the ion-track template approach combined with electrochemical deposition has been extensively applied to fabricate metallic, semiconductive, and conductive polymeric NWs in virtue of its simplicity and versatility. By this method, diameter (>10 nm), length (~um), shape (cylindrical, conical, rhombic, etc.), aspect ratio (tens to tens thousands), and areal density (single to 10^{10} cm^{-2}) of NWs can be controlled by template structural parameters, heavy ion irradiation, and chemical etching of ion tracks.[21,24,33] Besides, the control over crystallinity and crystallographic orientation of NWs has also been achieved.[21,24,33-35]

Gold possesses excellent electrical and thermal conductivities, high ductility, and chemical inertness, which fuels a wave of research on gold NWs.[3,7,31,36] For instance, gold NWs have shown very large yield strength than that of bulk nanocrystalline gold (~ 100 times).[1] The nanomembranes made of ultrathin gold NWs of 2.5 nm in diameter are mechanically strong, optically transparent and electrically conductive, showing promising applications in future lightweight foldable optoelectronics.[9] The highly crystalline gold NWs with atomically smooth surfaces show near-bulk conductivity and can serve as potential interconnects for future nanocircuits.[37] The [111]-oriented ultra-twinned gold NWs exhibit near-ideal theoretical strength where crystallographic orientations have a significant influence on their mechanical properties.[38] Single-crystal gold NWs have displayed periodic magnetoresistance oscillations induced by superconducting vortices.[39] Molecular dynamics simulations have revealed that structural transition and melting of gold NWs are highly dependent on crystallographic orientations.[17] Clearly, both crystallinity and crystallographic orientation can greatly influence the physicochemical properties of gold NWs.

Compared with extensive studies focusing on the various novel properties and micro-manipulation techniques and applications of gold NWs, less attention has been devoted to controlled fabrication of gold NWs. Using different electrolytes, pore sizes, and other fabrication conditions, gold NWs featured with different crystallinity and crystallographic orientation have been reported by different research groups.[21,24,33-35,40] Namely, single-crystal gold NWs were favored to grow when gold cyanide electrolytes were used[1,24,40] and the polycrystal structure have been usually achieved by using gold sulfite electrolyte.[23] For crystallographic orientation, using a cyanide electrolyte (Doduco), gold NWs with preferential orientation along [110] direction was obtained under potentiostatic

deposition and the preferential orientation changed to [100] direction when a reverse pulse deposition was used.[24,33] Furthermore, [111] crystallographically oriented gold NWs were also achieved by using a cyanide-based electrolyte provided by a different company (Orotemp).[41] It is clearly seen that the structural properties of electrochemically deposited gold NWs are highly dependent on electrolyte and other fabrication conditions. The aforementioned findings have been reported by different research groups at different conditions (electrolytes, pore diameters, applied voltages, deposition temperatures, etc.), which makes it difficult to generalize conditions under which desired structural characteristics can be obtained. Therefore the challenge to systematic control over crystallinity and crystallographic orientation of gold NWs is still open. More importantly, the electrolytes which have been widely adopted to electrochemically fabricate gold NWs are based on cyanide.[1,24,33,41-43] As well known, the cyanide is extremely toxic and environment-hostilely, especially at high temperatures (50-70 ℃).[44] Currently, the environment-friendly fabrication based on cyanide-free electrolytes represents a development trend of controlled fabrication of gold NWs.

In the present work, an environment-friendly method for fabrication of gold NWs with controlled crystallinity and crystallographic orientation is reported. The crystallinity and crystallographic orientation are systematically investigated with respect to fabrication conditions such as applied voltage, electrodeposition temperature and nanopore diameter. Furthermore, possible mechanisms of influences of those parameters on structural properties are discussed. In the end, we show that the preferred crystallographic orientation can dramatically enhance the field emission performance of the gold nanowires.

2. Experimental details

The process of synthesizing gold NWs consists of several steps. First, polycarbonate foils (Makrofol N, Bayer Leverkusen) of thickness 30 μm were irradiated at the UNILAC linear accelerator of GSI (Darmstadt, Germany) with 11.4 MeV/u $^{238}U^{28+}$ ions and at the Heavy Ion Research Facility at Lanzhou (HIRFL) with 9.5 MeV/u $^{209}Bi^{31+}$ ions at normal incidence. The irradiation fluence was 1×10^9 ions/cm^2. After irradiation, each side of the polymer foils was exposed to ultraviolet light for 2 hours to enhance track etching rate. This process, namely track sensitization, is necessary to produce highly cylindrical nanopores. In a next step, the membranes were chemically etched in a 5 M NaOH solution at 50 ℃ for a time from 0.5 to 4 minutes to obtain cylindrical pores with diameters ranging from 15 to 85 nm. During the etching process, an ultrasonic field was applied to achieve homogeneous etching. Immediately after etching, the foils were washed with distilled water in an ultrasonic field to remove residual NaOH solution, especially those in ion-track pores, avoiding excess etching. Subsequently, a thin gold film was sputtered onto one side of the foils and reinforced electrochemically by a Cu layer with a thickness of several micrometres. This backing layer served as cathode, and a gold bar with a diameter of 2 mm served as anode during the following electrochemical deposition of wires. Gold NWs with different diameters were prepared by direct current electrochemical deposition at varied electrodepositing voltages and temperatures. The employed electrolyte was aqueous solution of $Na_3Au(SO_3)_2$ (75g/L) which is more environment-friendly compared with cyanide-based counterparts. The deposition processes were monitored by recording curves of deposition current versus time and stopped until wire caps formed atop the membrane surface to ensure that the nanopores were entirely filled. The texture of gold NWs arrays were characterized by X-ray diffraction (XRD, RIGAKU D/Max-2400, Cu Kα, λ = 0.15406 nm) while NWs remained embedded in the templates. To make these examinations, both the wire caps and backing layer were removed. After dissolving the polymer membrane by dichloromethane (CH_2Cl_2), the morphology and crystallinity of gold NWs were examined by scanning electron microscopy (SEM, FEI NanoSEM 450), high resolution transmission electron microscopy (HRTEM, FEI Tecnai G2 F20) and selected area electron diffraction (SAED). The field emission characteristics of the nanowires were measured in a vacuum chamber with a base pressure below 1×10^{-5} Pa. The measurements were conducted on a standard parallel-plate-electrode configuration where a stainless-steel plate was used as the anode, and each sample was fixed onto a copper stage which served as the cathode. The distance between the nanowire tip and the anode was 300 μm. The *I-V* (current-voltage) curves were recorded by a computer-controlled measurement system.

3. Results and discussion

The gold in the aqueous solution is in the form of gold sulphite complex. During the electrochemical deposition of gold nanowires, the discharge of the gold sulphite complex consists of the following two steps:[45]

$$Au(SO_3)_2^{3-} \rightarrow AuSO_3^- + SO_3^{2-} \quad (1)$$

$$AuSO_3^- + e \rightarrow Au + SO_3^{2-} \quad (2)$$

The SEM image of a typical polycarbonate template shown in Figure 1(a) indicates that the nanopores are uniform in diameter, which ensures the fabricated NWs possessing a circular cross-section and narrow diameter distribution. The Figure 1(b) shows the optical microscopy image of a polycarbonate template with NWs embedded in it. The uniform color of template resulted from SPR (Surface Plasmon Resonance) signifies that the NWs evenly distribute in the template.[2] Dissolving the template matrix, the morphological characteristics of Au NWs with diameter of 75 nm

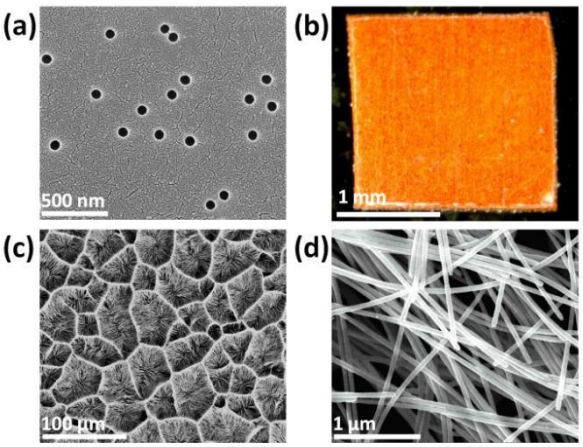

Fig. 1 (a) SEM image of a polycarbonate template with nanopore diameter of 75 nm. (b) Optical microscopy image of a polycarbonate template with NWs embedded in it. (c) & (d) show the SEM images of the as-prepared gold NWs at low and high magnifications, respectively.

diameter were investigated by SEM. For preparation of this sample, the deposition temperature and the applied voltage were kept to be 50 ℃ and 1.1 V, respectively. The low-magnification SEM image shown in Figure 1(c) demonstrates that the NWs are homogenously distributed on the backing layer and aggregated after dissolving the template matrix. Because the wire length equals to the template thickness of 30 μm, the aspect ratio of the NWs is expected to be as high as 400. The aggregation effect can be ascribed to the high aspect ratio, high ductility of gold and surface tension effect of solvent droplets when drying samples.[46] The high-magnification SEM image in Figure 1(d) displays that each wire has a cylindrical shape and that the wire diameter is uniform along the length direction.

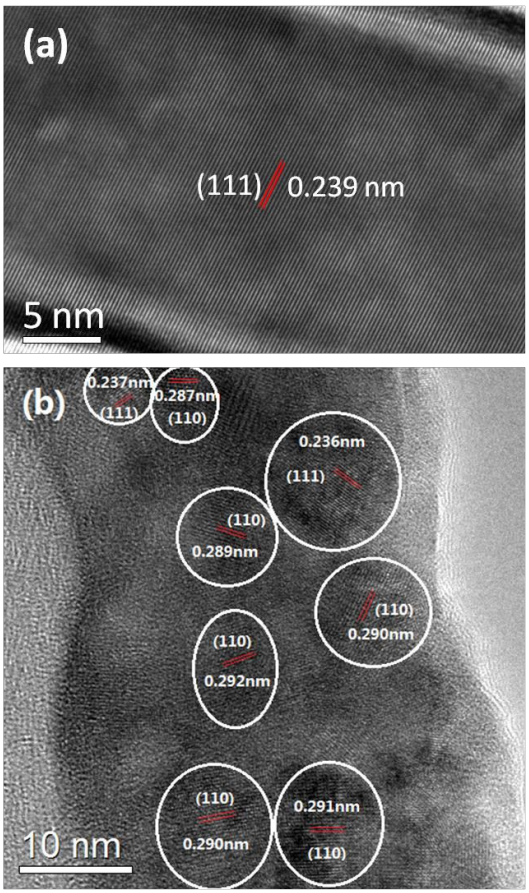

Fig. 2 HRTEM images of gold NWs fabricated at 50 °C. (a) single-crystal, applied voltage was 0.9 V; (b) polycrystal, applied voltage was 2.5 V.

HRTEM is widely employed to characterise crystallinity of materials. In this work, using HRTEM, we have checked the crystallinity of gold nanowires for several micrometres along the wires' length. If there is no grain boundary and only lattice fringes can be clearly observed, we conclude that they are single-crystal. As comparison, for poly-crystal wires, we have observed some small grains with different crystallographic orientations. For each sample, we have checked several wires to confirm their crystallinity. Figure 2 shows the HRTEM images of single-crystal and polycrystal NWs deposited at applied voltages of 0.9 V and 2.5 V, respectively, under deposition temperature of 50 ℃. The single- and poly-crystal structures were clearly illustrated by the images. As shown in Figure 2(a), the lattice fringes line up along wire length and the lattice spacing was measured to be 0.239 nm, corresponding to the (111) plan of face-centred cubic Au. We checked several micrometres along the wire length and no grain boundaries were observed. These results demonstrate that the wire possesses single-crystal structure. By comparison, in Figure 2(b), the lattice fringe spacing and orientation vary for different crystal grains designated by white circles and they are arranged orderly with each grain, which indicates a polycrystalline structure.

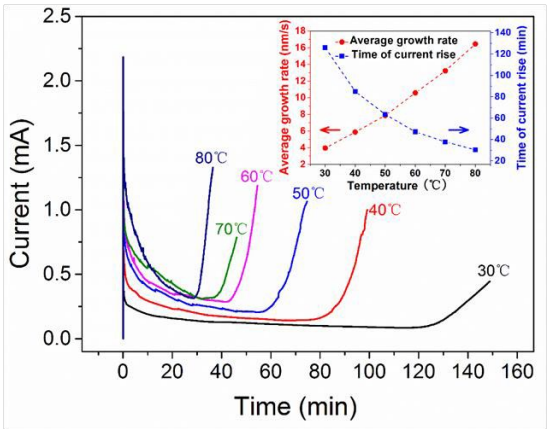

Fig. 3 Current-time curves for NWs deposited at different temperatures at 1.3 V. The inset shows average growth rate and time of current rise versus temperature for these wires.

The electrochemical deposition is an intricate process that can be affected by many factors. Accordingly, the crystal structure of metal NWs synthesized by template-assisted electrochemical deposition is significantly influenced by deposition conditions and growth dynamics. The formation of single-crystalline and polycrystalline structures of Au NWs can be ascribed to 2D layer-by-layer epitaxial mechanism and 3D nucleation-coalescence growth mechanism, respectively.[34,41,47,48] According to these two mechanisms, new grains will appear when the size of an initial cluster exceeds critical dimension N_c during deposition process. A larger N_c favours the single-crystal growth of NWs from an initial seed grain.[41,48] For 2D growth, N_c is expressed as

$$N_c = \frac{bs\varepsilon^2}{(ze\eta)^2} \quad (3)$$

where s, ε, z, e, η and b are the area occupied by one atom on the surface of nucleus, the edge energy, the effective electron number, elementary charge, the overpotential and a constant, respectively. The overpotential η is defined as the difference of external current induced potential E_i and equilibrium potential of electrode E_0 ($\eta = E_i - E_0$). For 3D growth, N_c is expressed as

$$N_c = \frac{8BV_m^2\sigma^3}{27(ze|\eta|)^3} \quad (4)$$

where V_m, σ and B are the volume occupied by one metallic atom on the surface of nucleus, the surface energy and a constant, respectively. A low applied voltage corresponds to a low overpotential η. In accordance with formula (3) and (4), the lower the η, the larger the critical dimension N_c. Namely, the low applied voltage favours single-crystal growth of NWs. With increasing applied voltage, N_c decreases and 3D clusters tend to grow independently of each other, coalesce and ultimately form polycrystalline NWs. These analyses are in good agreement with

our experiment results shown in Figure 2.

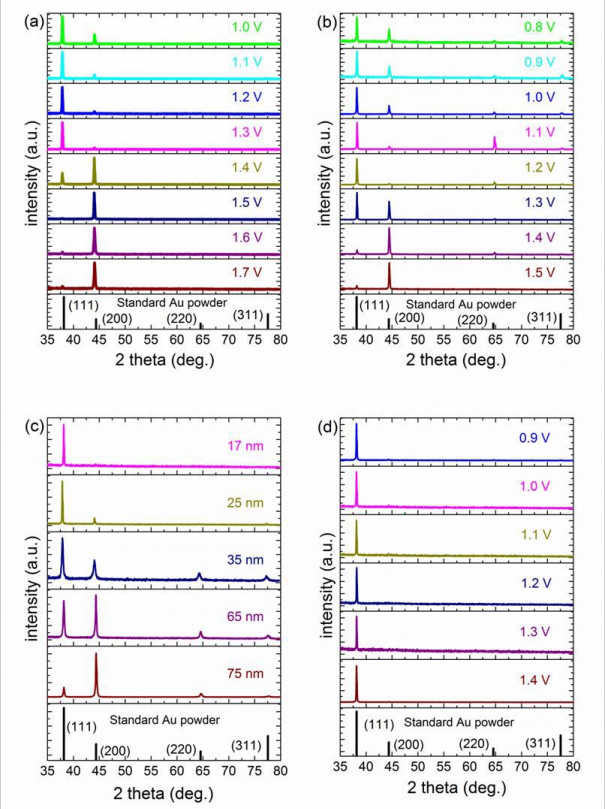

Fig. 4 XRD patterns of Au nanowire arrays synthesized at different conditions (nanopore diameter, applied voltage and deposition temperature): (a) 25 nm, 1.0 - 1.7 V, room temperature; (b) 25 nm, 0.8 - 1.5 V, 50 ℃; (c) 17 - 75 nm, 1.1 V, room temperature; (d) 17 nm, 0.9 - 1.4 V, room temperature.

It should be mentioned that higher deposition temperature not only promotes surface diffusion of atoms and thus favours 2D-like nucleus, but also accelerates the growth rate of wires, which hinders 2D growth.[41] The previous studies showed that a high overpotential may give rise to the surface adsorption of H ions or micelles in the electrolyte and thus considerably enhance the electrochemical reaction driving force which increases the deposition rate of metallic ions during electrodeposition.[34] Fast growth rate of NWs makes atoms difficult to diffuse freely and thoroughly and therefore to form polycrystalline structure. At a lower overpotential, it is easy to reach a steady diffusing process which favors single-crystal growth. However, due to the constraint of driving force, metallic ions cannot be deposited in pores if applied voltage is too low. In template-based electrochemical deposition of NWs, the growth progress can be monitored by current-time curve.[49] The current rises sharply as wires reach the top surface of the template and the average growth rate is calculated as the ratio of template thickness and the time of current rise. In our experiments, as shown in the inset of Figure 3, the time of current rise decreases dramatically and the average growth rate increases by four times when temperature increases from 30 ℃ to 80 ℃. Besides, NWs can continue to grow at lower overpotential in the presence of temperature filed. That is, high temperature can also enhance electrochemical reaction driving force. For single-crystal growth, the presence of temperature filed increases the growth rate of NWs, but promotes the surface diffusion of atoms and reduces the minimum applied voltage required to grow wires, resulting in a lager N_c. For poly-crystal growth, the enhancement of growth rate caused by high overpotential and high temperature promotes 3D nucleation although high temperature can improve the ion diffusion thereby impede 3D nucleation.

In addition to crystallinity, the preferential growth orientation of deposited NWs is found to be dependent on deposition conditions. Figure 4(a) shows that the XRD spectra for the NWs of 25-nm diameter deposited at room temperature under applied voltage from 1.5 to 1.7 V exhibit a single peak corresponding to the (200) crystalline plane, indicating that the NWs possess a well-preferred growth orientation along [100] direction. With decreasing the applied voltage to 1.3 V and lower, the NWs have a strong [111] orientation that dominates over the [100] orientation. At an elevated temperature 50 ℃, the orientation has a similar transition and the turning occurs at 1.4 - 1.2 V as shown in Figure 4(b).

In the present work, the NWs are deposited on the sputtered gold films which are polycrystalline. As reported previously, the polycrystal gold substrate has no effect on the preferential growth orientation of NWs.[27,35,48] In this case, in the initial stage of the wire growth, the crystallographic orientation of individual nuclei is random.[50] From the energy point of view, grains with lower surface energy grow faster than that with higher surface energy. The competition between adjacent crystal grains is inevitable because of the spatial restriction effect of the nanopores. Once a grain with preferential growth orientation survives, the consequent growth will be along this direction and form a single-crystal wire, according to the 2D growth mode. The transition length from 3D growth to 2D growth greatly depends on deposition conditions.[50] If the conditions weight against 2D nucleation, the NWs will grow under the 3D nucleation mode all the time and possess a poly-crystal structure.

The surface energy of Au crystal decreases in sequence for (220), (200), and (111) planes, and thus the (111) plane is more likely to appear during deposition. However, as reported previously, the surface energy of crystalline plane can be highly influenced by adsorption of H ions in electrolytes and a high applied voltage may make H ions appear on the cathode and thereby promote their adsorption.[34,51] Compared with intrinsic low-surface-energy planes, high-surface-energy planes are more preferable for the adsorption of H ions to meet the principle of minimum free energy. This adsorption could make the surface energy of crystal planes decrease and even lower than that of previous low-surface-energy planes.[21,47,48] The surface energy of the (220) plane is high such that the adsorption of H ions is not sufficient to make it possessing the lowest surface energy, but the (200) plane that has a relatively low surface energy can. Therefore, the NWs prefer to grow along [100] direction (perpendicular to the (200) plane) at higher voltage. Temperature could lower the voltage exhausted in electrolyte by accelerating the mobility of ions. Hence, the effective voltage at 50 ℃ is higher than that at room temperature when applying a constant voltage. That is why the voltage at which the growth direction of wires changes from [111] to [100] is lower at 50 ℃ than room temperature. In Figure 4(b), the relatively weak peak of (200) plane appears at low voltage and 50 ℃ because temperature causes the change of H adsorption and overpotential and thus disturbs the competition between (111) and (200) planes, but at

higher voltage the effect of adsorption is dominant and refrains that of temperature. Figure 4(c) displays the XRD patterns of the NWs with different diameters deposited at voltage of 1.1 V at room temperature. The NWs with diameters of 17 and 25 nm have well-preferred orientation along [111] direction. With increasing the NW diameter, the relative intensity of the diffraction peak corresponding to (111) plane gradually bates and that of (200) plane heightens. When the diameter reaches 75 nm, a strong preferred orientation along [100] direction is observed. It is interesting that, as shown in Figure 4(d), the NWs of 17-nm diameter deposited at 0.9 - 1.4 V at room temperature all possess a well-preferred [111] orientation and this preferential orientation is also observed for the NWs of the same diameter but deposited at 50 ℃ under a similar voltage range (results not shown here). These results can be ascribed to the effect of interface energy. In the electrochemical deposition, the growth of metallic nanowires is a complex process, which is influenced by factors such as charges transfer, ions diffusion, and H ions or micells absorption. However, from the energy point of view, crystal plane with low interface energy has more chances to be deposited to meet the principle of minimum free energy. The total interface energy includes two parts: wire top surface/electrolyte and side surface of wire/polycarbonate nanopore wall. At small diameters, the interface energy of top surface of wire/electrolyte gives less contribution to the total energy and in this case the total energy is mostly influenced by the side interface. Therefore, the most densely packed (111) plane has the lowest energy and thus has more possibilities to appear. At large diameters, the interface energy of top surface of wire/electrolyte has more contribution to the total energy and it is influenced by parameters such as voltage and temperature. Accordingly the crystallographic orientation can be controlled by these parameters.

In the end, the field emission performance of an array of vertically standing gold nanowires was measured. Figure 5(a) shows the measured *I-V* curve, i.e. emission current density *J* versus applied electric field *E*. The turn-on field of the array is 6.3 V/μm which is comparable to the reported value of 6.3 V/μm for gold nano-urchin and significantly lower than that for gold nanothorn (13.3 V/μm).[52] The field emission property is further analyzed by the Fowler-Nordheim (F-N) theory which is expressed as:[53,54]

$$ln\left(\frac{J}{E^2}\right) = ln\left(\frac{A_E\beta^2}{\phi}\right) - \frac{B_E\phi^{\frac{3}{2}}}{\beta E} \quad (5)$$

where $A_E = 1.54 \times 10^{-6}$ A·eV·V^{-2}, $B_E = 6.83 \times 10^3$ eV$^{-3/2}$·μm^{-1}, *J* is the current density, β is the field enhancement factor, *E* is the applied field, and ϕ is the work function of the emitter material (5.00 eV for Au[52]). As shown in the inset of Figure 5(a), the linear relationship of ln(J/E^2) versus 1/*E* indicates that the electron emission from the gold nanowires follows the F-N behaviour, i.e. a process of tunnelling of electrons through a potential barrier. According to formula (5), the field enhancement factor is deduced to be 281. It is well known that the enhancement of field emission generally results from local electric field enhancement at structure apex of protrusion. For a protrusion on a flat plane, the enhancement factor β may be expressed as $\beta = h/r$, where *h* is the height of the tip and *r* is the radius of curvature of the tip apex.[54] In the present work, the SEM image of the gold nanowire array for the field emission measurement is displayed in Figure 5(b). The

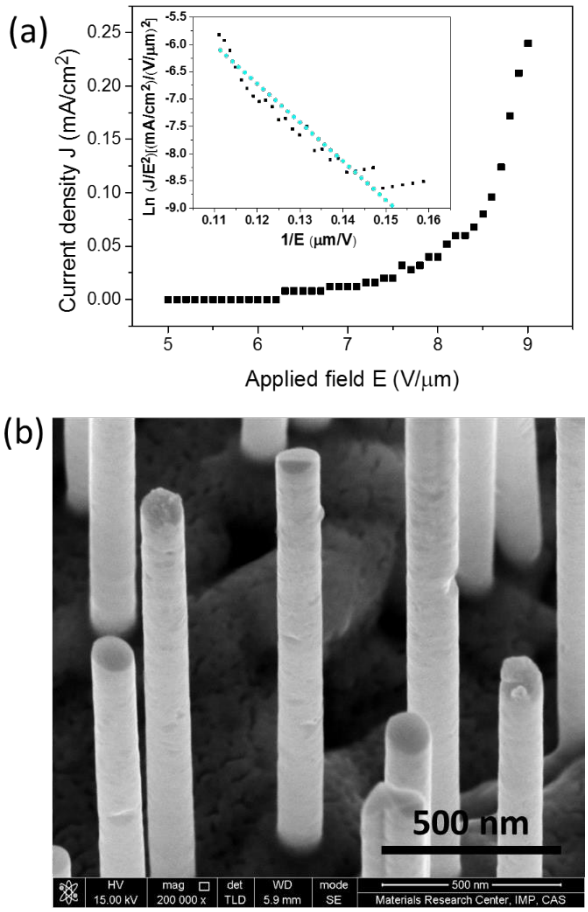

Fig. 5 Field emission J-E curve (a) and SEM image (b) of vertically standing gold nanowires. The inset in (a) is the corresponding F-N plots.

height and the diameter of the nanowires are approximately 2 μm and 120 nm, respectively. Therefore, the enhancement factor is calculated to be 33, which is significantly lower than the value of 281 extracted from the field emission measurement. The enhancement may be attributed to the crystallographic nature of the gold nanowires, i.e. single-crystal and [100] preferred orientation. On the one hand, it is notable in Figure 5(b) that the tips possess single-crystal features consisting of crystal facets rather than a single flat plane. Consequently, some sharp ridges are formed at the conjunctions of crystal facets and these ridges are essentially small protrusions where the local electric field is dramatically enhanced to facilitate the field emission process. On the other hand, it has been reported that different crystal planes have different work functions[55,56]. For materials including gold[55] and aluminium[56], loosely packed planes have lower work functions than closely packed planes and polycrystal gold. In this work, the gold wires for field emission measurement has preferred orientation along [100] direction. Therefore, the relatively lower work function could be the other contribution to the enhanced field emission.

Conclusions

In summary, by using a cyanide-free electrolyte, we have synthesized gold nanowires and its crystallinity and preferred

orientation can be controlled by tuning deposition conditions. While the applied voltage determines the crystal structure in a straightforward manner, the deposition temperature can have either restriction or promotion effect in the final crystal structure depending on the nanopore diameter of the ion track-etched template. We have also found that the growth orientation of the nanowires has a transition from [111] to [100] and the turning point depends on the applied voltage and nanopore diameter. These observations can be well explained by the adsorption of H ions modulated by effective voltage and the nanopore diameter-determined interface energy. Single-crystal wires with [100] preferred orientation shows enhanced field emission which may be attributed to their single-crystal structure and lower work function of loosely packed crystal plane.

Acknowledgments

We thank the members of the Materials Research Department at the GSI Helmholtz-Zentrum (Darmstadt, Germany) for preparation and irradiation of polycarbonate foils. The financial supports from the National Natural Science Foundation of China (Grant Nos.: 11175221, 11304261, 11375241, 11179003, 11275237, and 11205215) and the Hong Kong Research Grants Council (ECS Grant no. 509513) are acknowledged.

Notes and references

[a] *Materials Research Center, Institute of Modern Physics, Chinese Academy of Sciences, Lanzhou 730000, P. R. China.*
[b] *University of Chinese Academy of Sciences, Beijing, P. R. China*
[c] *Department of Applied Physics, The Hong Kong Polytechnic University, Hong Kong, P. R. China*
Email: j.liu@impcas.ac.cn (JL); j.duan@impcas.ac.cn (JLD)

1 B. Wu, A. Heidelberg and J. J. Boland, *Nat. Mater.*, 2005, **4**, 525-529.
2 H. Chen, L. Shao, Q. Li, J. Wang, Chem. Soc. Rev. 2013, 42, 2679-2724.
3 B. L. Wang, S. Y. Yin, G. H. Wang, A. Buldum and J. J. Zhao, *Phys. Rev. Lett.*, 2001, **86**, 2046-2049.
4 K. Gall, J. K. Diao and M. L. Dunn, *Nano Lett.*, 2004, **4**, 2431-2436.
5 A. L. Payt, B. Wiley, Y. N. Xia, A. T. Chen, L. Dalton, *Nat. Nanotechnol.*, 2008, **3**, 660-665.
6 F. Patolsky, Y. Weizmann and I. Willner, *Nat. Mater.*, 2004, **3**, 692-695.
7 J. R. Krenn, B. Lamprecht, H. Ditlbacher, G. Schider, M. Salerno, A. Leitner and F. R. Aussenegg, *Europhys. Lett.*, 2002, **6**, 663-669.
8 A. Roy, T. Pandey, N. Ravishankar and A. K. Singha, *AIP Adv.*, 2013, **3**, 032131.
9 Y. Chen, Z. Ouyang, M. Gu and W. L. Cheng, *Adv. Mater.*, 2013, **25**, 80-85.
10 J. G. Wang, M. L. Tian, N. Kumar and T. E. Mallouk, *Nano Lett.*, 2005, **5**, 1247-1253.
11 L. L. Xing, Y. F. Hu, P. L. Wang, Y. Y. Zhao, Y. X. Nie, P. Deng and X. Y. Xue, *Appl. Phys. Lett.*, 2014, **104**, 013109.
12 Z. Y. Bao, X. Liu, J. Y. Dai, Y. C. Wu, Y. H. Tsang and D. Y. Lei, *Appl. Surf. Sci.*, 2014, **301**, 351-357.
13 H. Wei, F. Hao, Y. Z. Huang, W. Z. Wang, P. Nordlander and H. X. Xu, *Nano Lett.*, 2008, **8**, 2497-2502.
14 Z. Y. Bao, D. Y. Lei, R. B. Jiang, X. Liu, J. Y. Dai, J. F. Wang, H. L. W. Chan and Y. H. Tsang, *Nanoscale*, 2014, **6**, 9063.
15 W. P. Zhu, H. T. Wang and W. Yang, *Acta Mater.*, 2012, **60**, 7112-7122.
16 W. F. Zhou, G. T. Fei, X. F. Li, S. H. Xu, L. Chen, B. Wu and L. D. Zhang, *J. Phys. Chem. C*, 2009, **113**, 9568-9572.
17 Y. H. Wen, Y. Zhang, J. C. Zheng, Z. Z. Zhu and S. G. Sun, *J. Phys. Chem. C*, 2009, **113**, 20611-20617.
18 A. Ramazani, M. A. Kashi, V. B. Isfahani and M. Ghaffari, *Appl. Phys. A*, 2010, **98**, 691-697.
19 S. Karim, M. E. Toimil-Molares, W. Ensinger, A. G. Balogh, T. W. Cornelius, E. U. Khan and R. Neumann, *J. Phys. D: Appl. Phys.*, 2007, **40**, 3767-3770.
20 A. Ramazani, M. A. Kashi and G. Seyedi, *J. Magn. Magn. Mater.*, 2012, **324**, 1826-1831.
21 J. L. Duan, J. Liu, D. Mo, H. J. Yao, K. Maaz, Y. H. Chen, Y. M. Sun, M. D. Hou, X. H. Qu, L. Zhang and Y. F. Chen, *Nanotechnology*, 2010, **21**, 365605.
22 A. J. Yin, J. Li, W. Jian, A. J. Bennett and J. M. Xu, *Appl. Phys. Lett.*, 2001, **79**, 1039-1041.
23 A. Ponrouch, S. Garbarino, S. Pronovost, P. L. Taberna, P. Simon and D. Guay, *J. Electrochem. Soc.*, 2010, **157**, K59-K65.
24 J. Liu, J. L. Duan, M. E. Toimil-Molares, S. Karim, T. W. Cornelius, D. Dobrev, H. J. Yao, Y. M. Sun, M. D. Hou, D. Mo, Z. G. Wang and R. Neumann, *Nanotechnology*, 2006, **17**, 1922-1926.
25 D. Mo, J. Liu, H. J. Yao, J. L. Duan, M. D. Hou, Y. M. Sun, Y. F. Chen, Z. H. Xue and L. Zhang, *J. Cryst. Growth*, 2008, **310**, 612-616.
26 H. J. Yao, J. L. Duan, D. Mo, H. Y. Günel, Y. H. Chen, J. Liu and Thomas Schäpers, *J. Appl. Phys.*, 2011, **110**, 094301.
27 F. Maurer, J. Brötz, S. Karim, M. E. T. Molares, C. Trautmann and H. Fuess, *Nanotechnology*, 2007, **18**, 135709.
28 Y. N. Wang, W. T. Wei, C. W. Yang and M. H. Huang, *Langmuir*, 2013, **29**, 10491-10497.
29 S. Tian, H. J. Li, Y. L. Zhang, S. Y. Zhang, Y. J. Wang, J. C. Ren and X. F. Qiang, *J. Cryst. Growth*, 2013, **384**, 44-49.
30 J. E. Hujdic, A. P. Sargisian, J. R. Shao, T. Ye and E. J. Menke, *Nanoscale*, 2011, **3**, 2697.
31 H. Liu, X. M. Cao, J. M. Yang, X. Q. Gong and X. Y. Shi, *Sci. Rep.*, 2013, **3**, 1-6.
32 T. David, L. Roussel, T. Neisius, M. Cabie, M. Gailhanou and C. Alfonso, *J. Cryst. Growth*, 2013, **383**, 151-157.
33 S. Karim, M. E. Toimil-molares, F. Maurer, G. Miehe, W. Ensinger, J. Liu, T.W. Cornelius and R. Neumann, *Appl. Phys. A*, 2006, **84**, 403-407.
34 H. Y. Sun, X. H. Li, Y. Chen, W. Li, F. Li, B. T. Liu and X. Y. Zhang, *Nanotechnology*, 2008, **19**, 225601.
35 X. W. Wang, G. T. Fei, X. J. Xu, Z. Jin and L. D. Zhang, *J. Phys. Chem. B*, 2005, **109**, 24326-24330.
36 A. I. Yanson, G. Rubio Bollinger, H. E. V. D. Brom, N. Agraït and J. M. V. Ruitenbeek, *Nature*, 1998, **395**, 783-785.
37 K. Critchley, B. P. Khanal, M. L. Gorzny, L. Vigderman, S. D. Evans, E. R. Zubarev and N. A. Kotov, *Adv. Mater.*, 2010, **22**, 2338-2342.
38 J. W. Wang, F. Sansoz, J. Y. Huang, Y. Liu, S. H. Sun, Z. Zhang and S. X. Mao, *Nat. Commun.*, 2013, **4**, 1-8.
39 L. He and J. Wang, *Nanotechnology*, 2011, **22**, 445704 (5pp).
40 J. Burdick, E. Alonas, H. C. Huang, K. Rege and Joseph Wang, *Nanotechnology*, 2009, **20**, 065306.
41 M. L. Tian, J. G. Wang, J. Kurtz, T. E. Mallouk and M. H. W. Chan, *Nano Lett.*, 2003, **3**, 919-923.
42 M. Schneckenburger, M. Kelsch, P. A. V. Aken, G. Richter, J. P. Spatz and A. Rustom, *Small*, 2012, **8**, 3396-3399.
43 C. Ji and P. C. Searson, *J. Phys. Chem. B*, 2003, **17**, 4494-4499.
44 J. S. Chen, Y. M. Fang, Q. Y. Qiu, L. X. You and J. Song, *Green Chem.*, 2011, **13**, 2339-2343.
45 H. Honma and Y. Kagaya, *J. Electrochem. Soc.*, 1993, **140**, L135-L137.
46 J. L. Duan, J. Liu, H. J. Yao, D. Mo, M. D. Hou,Y. M. Sun, Y. F. Chen and L. Zhang, *Mater. Sci. Eng. B*, 2008, **147**, 57-62.
47 H. Pan, B. H. Liu, J. B. Yi, C. Poh, S. Lim, J. Ding, Y. P. Feng, C. H. A. Huan and J. Y. Lin, *J. Phys. Chem. B*, 2005, **19**, 3094-3098.
48 H. Pan, H. Sun, C. Poh, Y. P. Feng and J. Y. Lin, *Nanotechnology*, 2005, **16**, 1559-1564.
49 M. E. T. Molares, V. Buschmann, D. Dobrev, R. Neumann, R. Scholz, I. U. Schuchert and J. Vetter, *Adv. Mater.*, 2001, **13**, 62-65.
50 X. H. Huang, G. H. Li, G. Z. Sun, X. C. Dou, L. Li and L. X. Zheng, *Nanoscale Res. Lett.*, 2010, **5**, 1057-1062.
51 X. W. Wang, G. T. Fei, L. Chen, X. J. Xu and L. D. Zhang, *Electrochem. Solid St.*, 2007, **10**, E1-E3.
52 T.-K. Huang, H.-W. Huang, C.-Y. Lee and H.-T. Chiu, *J. Chin. Chem. Soc.*, 2012, **59**, 983-988.

53 D. Banerjee, S. H. Jo and Z. F. Ren, *Adv. Mater.*, 2004, **16**, 2028-2032.
54 N. S. Xu and S. E. Huq, *Mater. Sci. Eng. R*, 2005, **48**, 47-189.
55 G. V. Hansson and S. A. Flodstrom, *Phys. Rev. B*, 1978, **18**, 1572-1585.
56 R. M. eastment and C. H. B. Mee, *J. Phys. F: Metal Phys.*, 1973, **3**, 1738-1745.